



# Homopolymer and multi-block Diels-Alder polyphenylenes: Synthesis, physical properties, X-ray diffraction, and gas transport



Timothy Largier, Fei Huang, Chris J. Cornelius\*

Department of Chemical and Biomolecular Engineering, University of Nebraska-Lincoln, Lincoln, NE 68588-0643, United States

## ARTICLE INFO

### Keywords:

Homopolymer and multi-block polyphenylene  
Gas transport  
Fractional free volume  
Physical properties  
X-ray diffraction

## ABSTRACT

A gas transport and X-ray structural analysis is reported for a methylated poly(phenylene) (MPP) and non-methylated poly(phenylene) (PP) homopolymer, a random copolymer, and MPP-PP block copolymers synthesized using Diels-Alder chemistry. These highly rigid and aromatic polymers display  $T_g$ 's of 400 °C and 382 °C for PP and MPP. Multi-block copolymerization of PP and MPP had a significant effect on the spatial arrangement of polymer chains as revealed by changes in the X-ray diffraction amorphous peak. The membranes displayed a narrower fractional free volume (FFV) from 0.288 to 0.304. The gas permeability, solubility, diffusivity and selectivity data for He, H<sub>2</sub>, O<sub>2</sub>, CO<sub>2</sub>, N<sub>2</sub>, and CH<sub>4</sub> were determined for this polymer series. Gas permeability variation between PP and MPP was 1.5% for H<sub>2</sub> (134 Barrers) and 16% for N<sub>2</sub> (7.11 Barrers). However, the multi-block MPP-PP-B2 led to permeability increases between 22.4% for H<sub>2</sub> (164 Barrers) and 61.7% for N<sub>2</sub> (11.5 Barrers). This work reveals clear relationships between the ordering of the amorphous region and gas diffusivity and solubility. The permselectivity trade-off did not correlate well to gas kinetic diameter (KD), polymer chemistry or composition, and depended largely on the gas pair. This poly(phenylene) family displayed high permeability and moderate ideal gas selectivity that were near the upper bound. Permselectivity results are compared to polyphenylene oxide (PO), functionalized PO using (–NH<sub>2</sub> and –NO<sub>2</sub>), 6FDA-DABA, and 6FDA-mPDA.

## 1. Introduction

Many industrial processes require gas sequestration or purification by selective separation between molecules [1]. Polymeric membrane-mediated gas separation processes are low cost, energy efficient, and environmentally friendly versus traditional methods [2–6]. The greatest challenge facing membrane development is the need for a simultaneous increase in permeability ( $P$ ) and selectivity ( $\alpha$ ). This has inspired material research efforts seeking to improve the understanding of interrelationships among polymer chemistry, morphology, and gas permselectivity. High gas  $P$  can result from elevated fractional free volume (FFV), which reduces the required membrane area, and energy required for gas transport. Gas  $\alpha$  is closely related to molecule diffusion and solubility within the membrane. Although much work has been performed on material modification to fine tune gas transport properties, the relationship of permselectivity to amorphous polymer microstructure is still under investigation.

Wide-angle X-ray scattering (WAXS) is a useful tool for obtaining chain spacing distances within amorphous polymers, which offers information regarding conformational orientation and organization [7,8]. Structural WAXS studies have indicated considerable ordering in the amorphous state, with spacing highly impacted by side group size [9,10]. It is therefore unsurprising that strong

\* Corresponding author.

E-mail address: [ccornelius2@unl.edu](mailto:ccornelius2@unl.edu) (C.J. Cornelius).

correlations have been found between WAXS analysis of the amorphous phase, and gas  $P$  and/or  $\alpha$  [11–13].

FFV is a parameter related to cavity size, and it has been used to fine tune material permselectivity through various physical and chemical modifications. Rubbers exhibit high FFV due to large segmental mobility, which decreases with temperature until a critical minimum free volume. Glassy 6FDA polyimides are a class of polymers that have shown great promise in industrial gas separation applications. These materials display decreased FFV (0.175–0.255) and typically have low gas  $P$ , and high selectivity [14]. Polymer modifications have been performed to increase FFV in order to impact  $P$ , such as copolymerization [15], inorganic hybridization [16], and blends [17]. Alternatively, poly(phenylene oxide) has a FFV up to 0.392, which displays high gas permeability [18]. A 5% decrease in FFV via sulfonation doubled  $\text{CO}_2/\text{CH}_4$  selectivity with a marginal decline in  $P$ . Due to the ease of such modification, glassy aromatic polymers with high fractional free volumes are sought that lie near the permselectivity upper bound.

Diels-Alder poly(phenylene)s are highly amorphous and rigid polymers with elevated thermochemical and mechanical stability that have been under consideration for numerous applications [19–21]. The materials have exhibited surprisingly high flexibility due to meta- catenation and twisting conformations around the backbone [22]. In this paper an X-ray diffraction and gas transport analysis of methylated and non-methylated poly(phenylene) homopolymers and block copolymers are reported. The  $P$ , solubility ( $S$ ), diffusivity ( $D$ ), and  $\alpha$  data for He,  $\text{H}_2$ ,  $\text{O}_2$ ,  $\text{CO}_2$ ,  $\text{N}_2$ , and  $\text{CH}_4$  obtained for these membranes were correlated to gas KD and condensability, and an X-ray structural analysis.

## 2. Experimental

### 2.1. Materials

1,4-Diethynylbenzene (Fischer Scientific, 95%) was purified by sublimation prior to use. 1,3-Diphenylacetone (99%), acetone ( $\geq 99.5\%$ ), toluene ( $\geq 99.5\%$ ), tetrahydrofuran (99.9%) and methanol ( $\geq 99.8\%$ ) were purchased from Fisher Scientific and used as received. Dichloromethane (99.9%) and diphenyl ether (99%) were purchased from Acros Organics and used as received.

### 2.2. Polymer and copolymer synthesis and membrane formation

Poly(phenylene), methylated poly(phenylene), and block copolymers were synthesized via Diels-Alder polymerization, as reported elsewhere [23,24]. Bis(cyclopentadienone) monomers were synthesized in house, according to literature [24,25]. The described procedure is for the synthesis of the homopolymer poly(phenylene). Bis(tetraphenylcyclopentadienone) (15.00 g, 18.36 mmol), 1,4-diethynylbenzene (2.316 g, 18.36 mmol), and 125 mL of diphenyl ether was charged to a reaction vessel. The vessel was sealed, and the solution freeze-pump-thawed three times. The vessel was flooded with argon, and heated to 180 °C while stirred with a magnetic stir bar. The solution color typically changed from dark brown to orange after four hours; however, the reaction was allowed to continue for an additional 24 h in order to maximize molecular weight. Upon completion, the solution was diluted with toluene, and precipitated into acetone, to give the tan polymer poly(phenylene) (PP). A random copolymer was formed through a Diels-Alder reaction with molar equivalents of methylated and non-methylated bis(tetraphenylcyclopentadienone). To form block copolymers, blocks were synthesized in separate reactions, controlling molecular weight using Carother's equations. The blocks were then purified, analyzed, and subsequently copolymerized (Fig. 1).

The polymers and copolymers were dissolved in methylene chloride 2% by weight, and pipetted into a glass mold. The rate of solvent evaporation was controlled by covering the mold with a glass slip, allowing for film formation over a 24-h period. Films were then in a placed in an oven under vacuum overnight to ensure complete removal of solvent. The orange, transparent, and creasable films had thicknesses that were controlled to 85–90  $\mu\text{m}$ .

### 2.3. Material characterization

The molecular weights and their distributions were obtained using an Agilent 1260 GPC/SEC System with a TL105 HPLC column heater from Timeberline Instruments®. The system consisted of a series of two linear PSS® SDV columns, with a porosity of 1000 Å and 100,000 Å, giving a column combination separation range of 100–1,000,000 Da. A twelve point calibration curve, obtained within one day of data collection, was obtained using poly(styrene) standards with a molecular weight range of 474–2,520,000 Da from PSS® (PSS-pskitr1). The GPC was run with a tetrahydrofuran mobile phase, and a column temperature of 25 °C. The flow rate during operation was 1 mL/min, and an injection volume of 100  $\mu\text{L}$  was used. Samples were 0.1 wt.% and filtered through a 0.45  $\mu\text{m}$  PTFE filters.

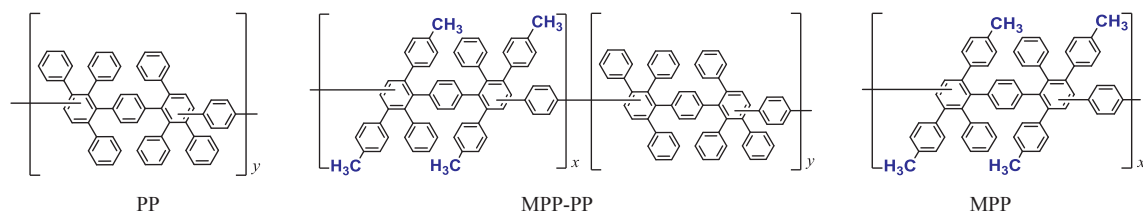


Fig. 1. Chemical structure of PP, multi-block MPP-PP, and MPP polymers.

In order to confirm complete polymerization and determine copolymer composition,  $^1\text{H}$  NMR analysis was performed using a Bruker Avance III-HD 400 MHz NMR. All materials were analyzed in  $\text{CD}_2\text{Cl}_2$ .

The thermal gravimetric analysis (TGA) studies were done to evaluate a polymer's thermal stability using a TA Instruments model Q500 Thermo Gravimetric Analyzer. A  $10\text{ }^\circ\text{C}$  per minute scan rate from  $50\text{ }^\circ\text{C}$  to  $700\text{ }^\circ\text{C}$  with a  $20\text{ mL}$  per minute  $\text{N}_2$  purge flow rate was used. Thin film samples were loaded between  $10$  and  $15\text{ mg}$ .

A TA Instruments DMA Q800 (Dynamic Mechanical Analysis) was used to characterize the glass transition temperature and molecular transitions of materials. All experiments were performed under  $\text{N}_2$ . In a typical run, a static force of  $0.010\text{ N}$  was applied and the temperature was equilibrated to  $40.0\text{ }^\circ\text{C}$ . The temperature was then ramped at  $1\text{ }^\circ\text{C}$  per minute to  $450\text{ }^\circ\text{C}$ . Thin film dimensions for these tests had a length of roughly  $10\text{ mm}$ , width of  $2.5\text{ mm}$ , and thickness of  $75\text{ }\mu\text{m}$ . In order to ensure a linear viscoelastic response, sample dimensions were set to ensure a length to width ratio of at least 3.

Differential Scanning Calorimetry (DSC) was used to assess polymer thermal transitions using a TA instruments DSC Q20. In a typical run, the temperature was increased from  $50$  to  $450\text{ }^\circ\text{C}$  at a ramp rate of  $1\text{ }^\circ\text{C}/\text{min}$  under nitrogen atmosphere. Each polymer was run twice to ensure accuracy.

Density ( $\rho$ ) measurements were performed by using a Mettler Toledo XS205 analytical balance. This instrument was fitted with a Mettler density determination kit, which is based on Archimedes' principle. Methanol was used as the auxiliary liquid.

The polymer's fractional free volume (FFV) was determined by measuring its specific volume  $V$  (i.e. the inverse of  $1/\rho$ ), and occupied volume  $V_o$  (Equation 1).

$$FFV = 1 - \frac{V_o}{V} = 1 - \frac{1.3 \sum_{k=1}^K (V_w)_k}{V} \quad (1)$$

$V_o$  was determined using group contribution method proposed by Bondi [26] where  $V_w$  is the van der Waals volume for each unique functional group contribution  $k$ , and the total number of structural groups  $K$  within the polymer. The van der Waals volumes used in this work are presented in Table 1.

Wide angle X-ray diffraction (WAXD) was performed on a Rigaku SmartLab Diffractometer ( $\text{Cu K}\alpha$ ,  $\lambda = 1.54\text{ \AA}$ ). Analysis was performed at  $40\text{ kV}$  and  $44\text{ mA}$ . A continuous scan was performed for a  $2\theta$  range of  $2\text{--}50^\circ$ , with a step of  $0.02^\circ$  at a scan speed of  $1^\circ/\text{min}$ . The scan covered a  $q$  range of  $0.14\text{--}3.51\text{ \AA}^{-1}$ , where  $q = 4\pi\sin(\theta/\lambda)$ . The d-spacing of the corresponding peaks were calculated by the equation  $d = 2\pi/q$ .

Gas transport properties were obtained using a custom-built gas permeation system that is ideally shown in Fig. 2. The system utilized the time-lag technique which was used to measure  $P$ ,  $D$ , and  $S$  [28]. Gases used in this study were He,  $\text{H}_2$ ,  $\text{O}_2$ ,  $\text{CO}_2$ ,  $\text{N}_2$ , and  $\text{CH}_4$  with a purity of  $99.999\%$  (ultra-pure, Matheson Tri-Gas®). All samples were  $80\text{--}90\text{ }\mu\text{m}$  in thickness, and were heated to  $220\text{ }^\circ\text{C}$  under vacuum for  $24\text{ h}$  prior to testing. Feed pressure and test temperature were preset and held constant at an absolute pressure of  $4\text{ atm}$  and  $30\text{ }^\circ\text{C}$ . The automated gas permeation testing process is controlled and programmed by LabVIEW graphical interface programming software. The reproducibility in measuring  $P$  was used to assess the relative error for this technique and was found to be  $5\%$ .

### 3. Results and discussion

#### 3.1. Molecular weight and composition

The poly(phenylene) homopolymers and block copolymers were analyzed using  $^1\text{H}$  NMR to determine polymer structure, and the fraction of methylated to non-methylated repeat units. As shown in Fig. 3 the  $^1\text{H}$  NMR spectra consisted of two regions of interest, aromatic protons evident from  $7.5$  to  $6.0\text{ ppm}$ , and a methyl proton triplet at  $2.5\text{--}2.0\text{ ppm}$ . The methyl triplet is attributed to irregularities in the regiochemistry of the polymer backbone due to the addition of  $1,4\text{-diethynylbenzene}$ . This produces isomers that have been observed in other studies involving MPP [19]. These regions were integrated in order to determine the fraction of methylated to non-methylated repeat units.

Block compositions and molecular weight distributions (MWD) of individual blocks and polymers are shown in Table 2. Previous reports have shown a strong dependence between MWD, reaction time, temperature, and concentration [29,30]. Although a composition of  $50\%$  methylated repeat units was desired for the random and block copolymers, the methylated composition was between  $44$  and  $53\%$ , which is likely due to the presence of impurities. Weight average molecular ( $M_w$ ) weights for all Diels-Alder polymerizations ranged from  $153,000$  to  $192,000$ . Polymer condensation reactions nominally have a polydispersity index (PDI) of  $2.0$ . A higher PDI of  $2.7$  was observed for MPP-PP-B1 that is due to a lower number-average molecular weight ( $M_n$ ), which signals a

**Table 1**  
Van der Waals volumes ( $V_w$ ) for various structural groups [27].

Group	$V_w$ ( $\text{cm}^3/\text{mol}$ )
Phenyl	45.85
Phenyl (para/meta)	43.3
Phenyl (pentasub.)	-4.6
$-\text{CH}_3$	13.67

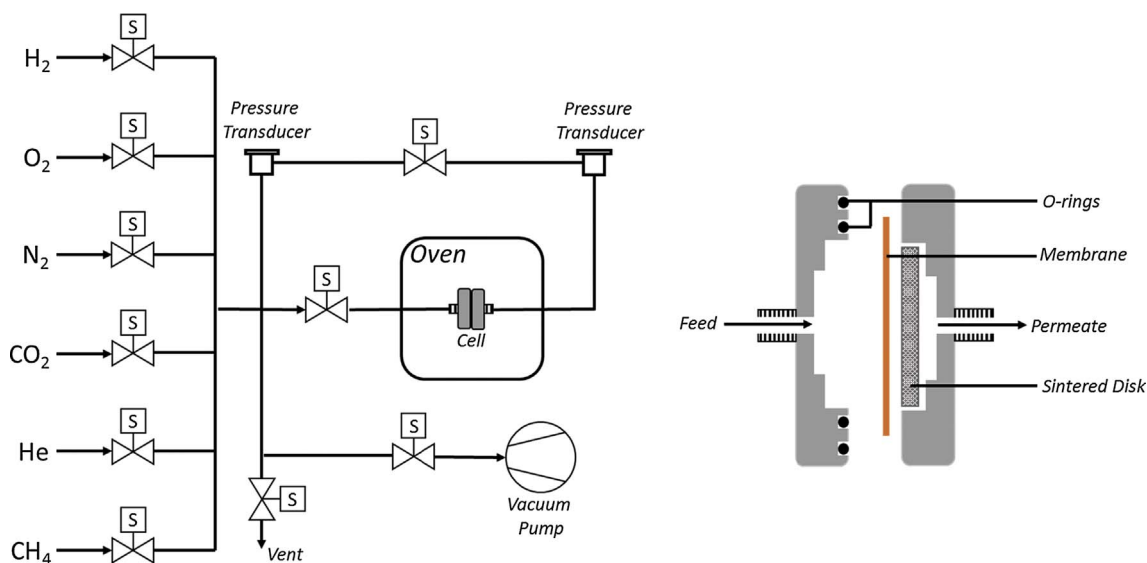


Fig. 2. Gas permeation set-up and gas permeation cell schematic representation.

larger concentration of oligomers.

### 3.2. Solubility, $\rho$ , and FFV

All the polymers discussed in this work displayed good solubility in a wide range of common organic solvents, including toluene, chloroform, and THF. Previous reports have attributed the high degree of solubility to polymer stereochemistry. In each [4 + 2]-cycloaddition two distinct regioisomers are possible which leads to the possibility of both para- and meta- couplings within the main polymer chain (Fig. 1). Stille and Noren, using a model reaction under similar conditions, reported that no more than 50% of meta-isomers were produced [29]. However, a later study concluded that 83% of isolated polymer was of the *m,m*-isomer [30]. Therefore the high degree of solubility has been attributed to meta-catenation, as well as significant twisted conformations that limit or block conjugation [22]. Meta linkages, reducing polymer symmetry and increasing entropy, have also been shown to decrease the glass transition temperature, a phenomenon that has been documented in other polymer systems [31,32].

PP, MPP, and MPP-PP estimated FFV was predicted using Bondi's group contribution method based upon their  $V$  and  $V_o$  (Eq. (1)).

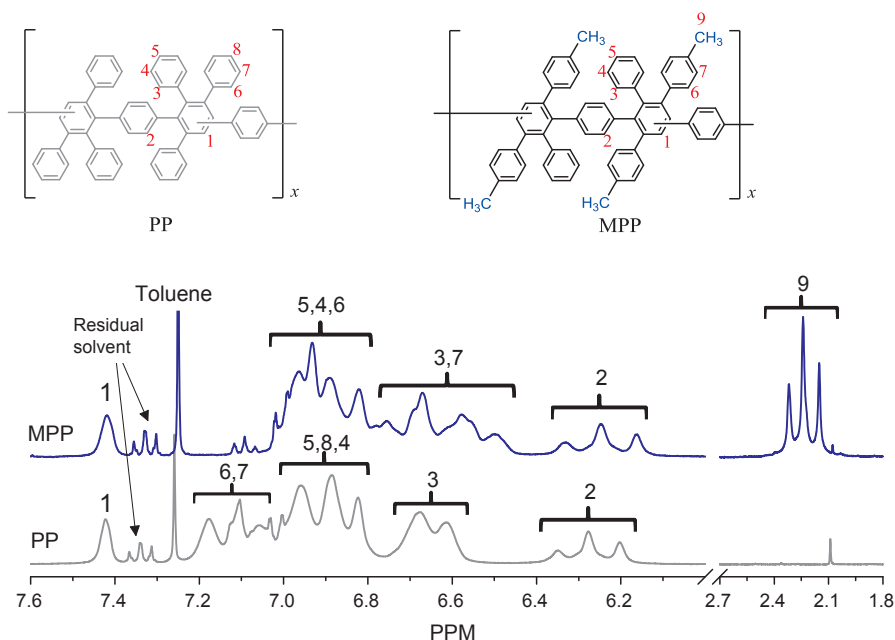


Fig. 3.  $^1\text{H}$  NMR spectra of poly(phenylene) (PP) and methylated poly(phenylene) (MPP).

**Table 2**  
Polymer molecular weight distributions and repeat unit compositions.

	$M_{nx}$ ( $10^3$ g/mol)	$M_{ny}$ ( $10^3$ g/mol)	Composition $f_{MPP}:f_{PP}$	$M_n$ ( $10^3$ g/mol)	$M_w$ ( $10^3$ g/mol)	PDI -
PP	–	–	0.00:1.00	78.7	192	2.4
MPP-PP-RC	–	–	0.44:0.56	75.2	153	2.0
MPP-PP-B2	16.8	16.3	0.44:0.56	76.2	175	2.3
MPP-PP-B1	11.2	8.87	0.53:0.47	56.4	154	2.7
MPP	–	–	0.96:0.04	89.9	180	2.0

Table 3 is a summary of the polymer's  $\rho$ ,  $V$ ,  $V_o$ , molar mass of its repeat unit ( $M$ ). The predicted FFV for PP (0.291) and MPP (0.301) lie between poly(sulfone) (0.156) and poly(phenylene oxide) (0.392) [33,34]. The FFV changes less than 5% between MPP-PP-B1 (0.288), MPP-PP-B2 (0.304), and MPP-PP-RC (0.299) versus PP and MPP. This suggests that using only FFV predictions may not accurately reflect all the physical and compositional changes occurring within these materials due to estimates associated with  $V_w$  and  $V_o$ . Therefore, in order to assess and compare dimensional changes within the material, the specific volume ( $V = 1/\rho$ ) will be used to discuss property variations. PP and MPP displayed the lowest and highest  $V$  of 646 and 738  $\text{cm}^3/\text{mol}$ . The random MPP-PP-RC copolymer's  $V$  lies between the homopolymers MPP and PP. However, despite similar chemical composition, it differs from the block copolymers MPP-PP-B1 and MPP-PP-B2. This increase in specific volume suggests that the methyl moiety, and increase in methyl block length disrupts chain packing, which leads to a void spacing increase between polymer chains.

### 3.3. Thermal transitions and degradation

The thermal transition of PP, MPP, MPP-PP-B1, MPP-PP-B2, and MPP-PP-RC were evaluated using DMA and DSC and summarized in Table 4. Diels-Alder poly(phenylene) DSC measurements has been shown to give poorly resolved curves [35]. Although this was observed for all polymers in this work, the second DSC run revealed a  $T_g$  for PP (390 °C) and MPP (365 °C). This result suggests that the methyl moiety within MPP leads to a disruption in chain packing, which enables greater segmental and chain mobility at lower temperatures. The random and block copolymer  $T_g$  increased with PP block length, which is proportional to changes in  $V$ .

PP, MPP, MPP-PP-B1, MPP-PP-B2, and MPP-PP-RC dynamic viscoelastic changes as a function of temperature are shown in Fig. 4. The  $T_g$ 's obtained using DSC and DMA differed by up to 20 °C. The loss modulus ( $E''$ ) of polyphenylene systems containing a methyl group displayed a broad and low temperature peak between 250 and 350 °C. This indicates a  $\beta$  relaxation, which is attributed to a segmental mobility mode not present within PP. Despite lower  $T_g$ 's, the methylated materials display far less chain relaxation in this region. It is assumed that the presence of the methyl moiety, despite reducing the  $T_g$  via disruption of chain packing, hinders segmental mobility by increasing the rotational energy barrier due to this side group. Although well below the degradation temperature, the methylated materials display a sharp upturn in storage modulus, as well as a second peak in the loss modulus at roughly 400 °C (Table 4). This indicates some degree of crosslinking, which is increased by the presence of the methyl moiety. To support this hypothesis, methylated polymers heated that had been briefly heated to 450 °C during a DSC test were no longer soluble in chloroform, and only swelled in it. This behavior has not yet been investigated and will be explored in future work.

TGA experiments were performed to determine material temperature stability (Fig. 5). All materials displayed a sharp and single degradation step. MPP had the lowest onset of degradation at 539 °C, and five percent weight loss ( $T_d^{5\%}$ ) that occurred at 552 °C. This result is attributed to methyl group instability at lower temperatures. However, the block copolymers displayed increasing stability with increasing block length. The onset of degradation for MPP-PP B1 and MPP-PP B2 was 576 and 569 °C. Finally, polyphenylene displayed the greatest stability, with an onset of degradation of 581 °C, and a  $T_d^{5\%}$  of 576 °C. The amount of residue (char) increased with the addition of the methyl moiety, from 67% for PP to 83–85% for the block copolymers. This observation further supports the evidence of crosslinking within the methylated materials, which is less stripping of volatiles and more char [36]. The degradation mechanism of this polymer chemistry is still under investigation.

### 3.4. X-ray scattering

The X-ray diffraction patterns for all materials, obtained by wide-angle X-ray scattering, are shown in Fig. 6, and summarized in Table 5. Despite only small changes in polymer chemistry, the homopolymers PP and MPP displayed significantly different X-ray

**Table 3**  
Polymer density ( $\rho$ ),  $V_o$ ,  $V$ , and FFV.

	$M$ (g/mol)	$\rho$ (g/cm <sup>3</sup> )	$V_o$ (cm <sup>3</sup> /mol)	$V$ (cm <sup>3</sup> /mol)	FFV	Composition $f_{MPP}:f_{PP}$
PP	761.0	1.178	458	646	0.291	0.00:1.00
MPP-PP RC	785.7	1.139	484	690	0.299	0.44:0.56
MPP-PP B2	785.7	1.130	484	695	0.304	0.44:0.56
MPP-PP B1	790.8	1.152	489	687	0.288	0.53:0.47
MPP	817.0	1.107	516	738	0.301	0.96:0.04

**Table 4**  
Glass transition and degradation temperatures.

	DSC T <sub>g</sub> (°C)	DMA T <sub>g</sub> (°C)	T <sub>d</sub> <sup>5%</sup> (°C)
PP	390	400 <sup>a</sup>	581
MPP	365	382	552
MPP-PP RC	379	384	601
MPP-PP B1	380	400	600
MPP-PP B2	384	403	589

<sup>a</sup> Polymer failure.

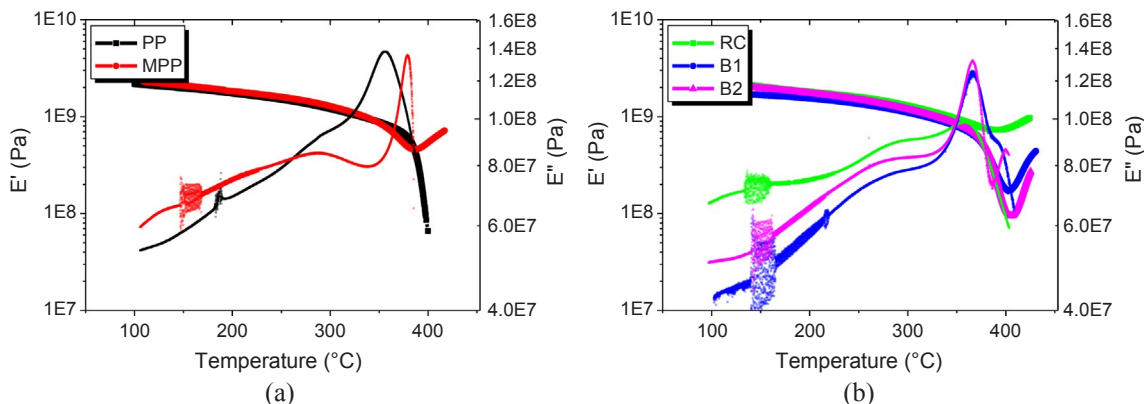


Fig. 4. The temperature effects upon (a) storage modulus ( $E'$ ) and loss modulus ( $E''$ ) of PP and MPP versus (b) RC and PP-MPP multi-blocks B1 and B2.

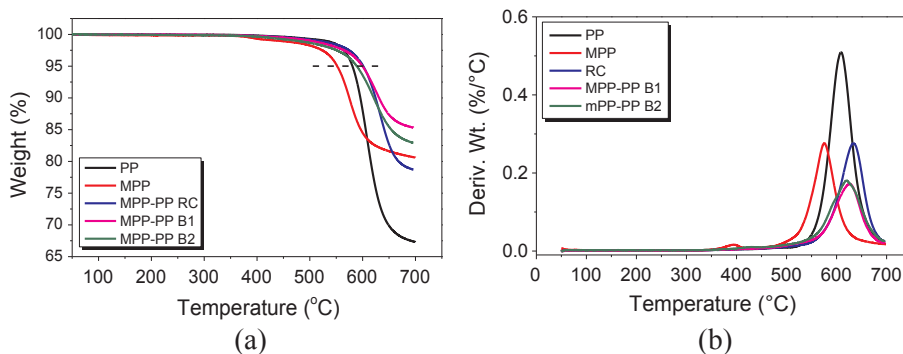


Fig. 5. Thermal gravimetric properties of PP, MPP, and PP-MPP multi-blocks.

spectra. Three peaks are evident, correlating to diffraction plane distances (d-spacing's) of roughly 11.2, 5.5, and 2.1 Å. Large peak breadths are the result of the amorphous nature of these materials. Peak d-2 is the pervasive “amorphous halo”, that is observed in polymer melts, glasses and rubbers. Peak d-1 has been most commonly observed in atactic polystyrene, and is referred to as the “polymerization peak” [37–39]. This peak is not observed in most glassy polymers, and despite great efforts it is still not well understood. In a molecular dynamics simulation of atactic polystyrene, peak contributions were determined that were in agreement with our experimental observations [40]. The study concluded that the “polymerization peak” (d-1) was the true amorphous peak, as it reflects inter-chain packing. The higher  $q$  peak (d-2) was found to be mainly due to side chain (phenyl-phenyl) correlations, while peak d-3 can be attributed to side chain intermolecular interactions.

In Fig. 7 the distance between diffraction planes (d-spacing) of the d-1 feature was plotted as a function of the methylated block-mer length,  $V$ , and FFV. This large feature is of particular interest as it suggests ordering in the amorphous region of the material. As previously discussed, the calculated FFV displays little variation between polymers, and therefore reveals no observable correlations. However, a strong relationship is observed between methylated-mer length, and d-spacing, which signifies the importance of both block length and chemistry. The amorphous feature is also well correlated to an increase in specific volume, indicating agreement between changes in the measured polymer  $\rho$  and the size of the amorphous feature. Future work would benefit from more accurate free volume characterization techniques such as positron annihilation [41,42]. Such an effort would allow one to develop better relationships between polyphenylene chemistry, void spacing, and microstructure.

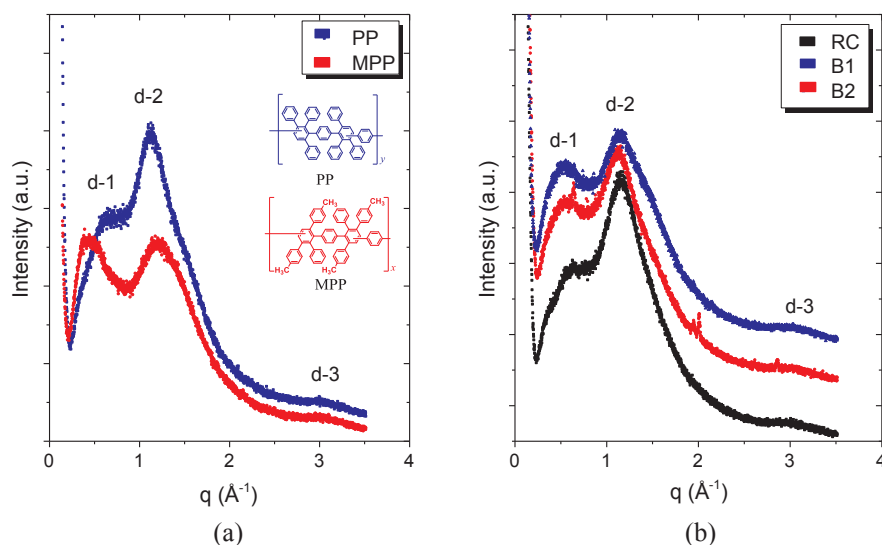


Fig. 6. X-ray diffraction patterns for the polymer membranes.

Table 5  
Polymer diffraction peaks.

	d-1 d-spacing (Å)	d-2 d-spacing (Å)	d-3 d-spacing (Å)
PP	9.60	5.6	2.1
MPP	14.1	5.2	2.1
MPP-PP RC	10.0	5.4	2.1
MPP-PP B1	10.8	5.6	2.1
MPP-PP B2	11.4	5.5	2.1

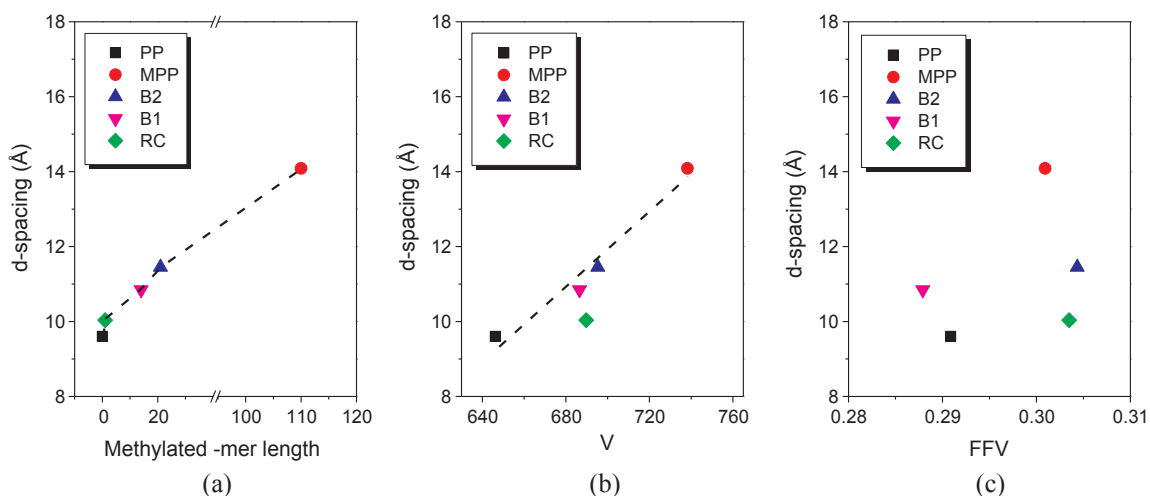


Fig. 7. The distance between diffraction planes (d-spacing) of the d-1 feature as a function of (a) methylated block –mer length, (b)  $V (1/\rho)$  and (c) FFV.

### 3.5. Effect of polymer chemistry and block length on gas $P$ and $\alpha$

Fig. 8 displays  $P$ ,  $D$ , and  $S$  as a function of gas KD. Gas  $D$  decreases with increasing KD, with the exception of  $\text{CO}_2$ . No trend appears to be evident between  $P$  and KD due to high  $\text{CH}_4$  and  $\text{CO}_2$  solubility within these polymers. Gas  $S$  within a membrane is typically a function of gas condensability, represented by its critical temperature ( $T_c$ ). A somewhat linear relationship is observed between  $S$  and  $D$  versus  $T_c$ , which provides a better explanation of observed gas transport properties.  $\text{CO}_2$  does appear to have an exceptionally high solubility relative to its condensability, which is likely due to molecular properties. Molecular interactions were found to have the largest impact upon gas solubility within these films, which is attributed to a gas binding enthalpy and an excluded

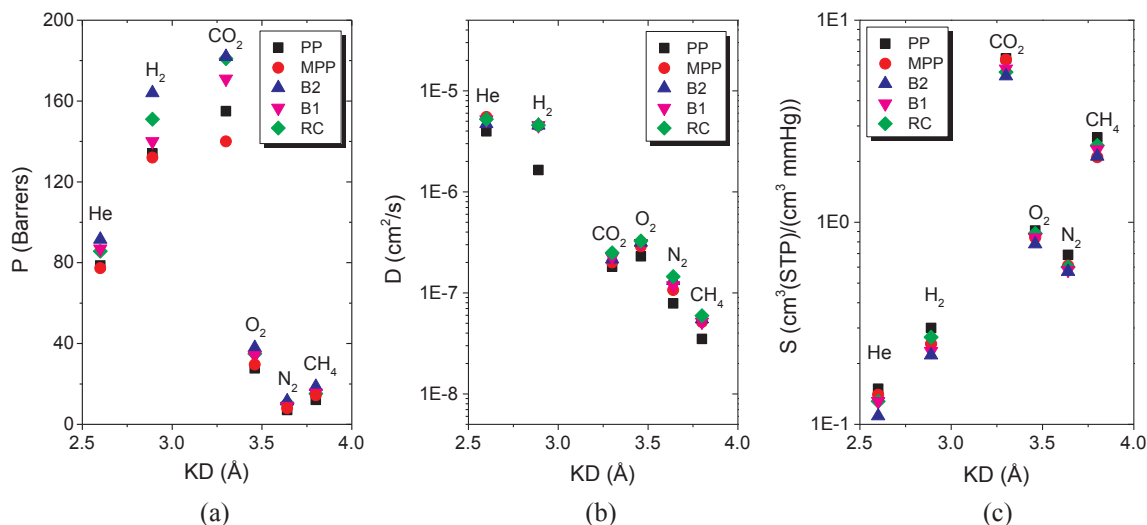


Fig. 8.  $P$ ,  $D$ , and  $S$  plotted as a function of  $KD$ .

Table 6

Gas permeabilities obtained at 25 °C and a feed pressure of 4 atm.

	He	H <sub>2</sub>	CO <sub>2</sub>	O <sub>2</sub>	N <sub>2</sub>	CH <sub>4</sub>
<i>Permeability (Barrer)</i>						
PP	78.6	134	155	27.7	7.11	12.1
MPP-PP RC	85.7	151	181	34.9	10.5	15.2
MPP-PP B2	91.5	164	182	37.9	11.5	18.7
MPP-PP B1	86.9	140	171	34.1	9.07	15.6
MPP	77.3	132	140	29.6	7.97	14.4
<i>Diffusivity * 10<sup>8</sup> (cm<sup>2</sup>/s)</i>						
	He	H <sub>2</sub>	CO <sub>2</sub>	O <sub>2</sub>	N <sub>2</sub>	CH <sub>4</sub>
PP	398	346	18.2	23.1	7.87	3.51
MPP-PP RC	471	455	21.5	31.6	13.2	5.51
MPP-PP B2	523	458	24.9	32.6	14.5	5.95
MPP-PP B1	518	454	22.6	31.0	11.9	5.16
MPP	551	452	20.0	29.0	10.7	5.16
<i>Solubility (cm<sup>3</sup> (STP)/cm<sup>3</sup> atm)</i>						
	He	H <sub>2</sub>	CO <sub>2</sub>	O <sub>2</sub>	N <sub>2</sub>	CH <sub>4</sub>
PP	0.15	0.30	6.47	0.91	0.69	2.63
MPP-PP RC	0.14	0.25	6.38	0.84	0.61	2.10
MPP-PP B2	0.13	0.27	5.54	0.88	0.60	2.40
MPP-PP B1	0.13	0.23	5.75	0.84	0.58	2.29
MPP	0.11	0.22	5.29	0.78	0.57	2.12
<i>Ideal selectivity</i>						
	CO <sub>2</sub> /CH <sub>4</sub>	O <sub>2</sub> /N <sub>2</sub>	CO <sub>2</sub> /N <sub>2</sub>	H <sub>2</sub> /N <sub>2</sub>	He/CH <sub>4</sub>	He/N <sub>2</sub>
PP	12.7	3.9	21.7	18.9	6.5	11.1
MPP-PP RC	11.9	3.3	17.1	14.3	5.6	8.1
MPP-PP B2	9.7	3.3	15.8	14.2	4.9	7.9
MPP-PP B1	11.0	3.8	18.9	15.4	5.6	9.6
MPP	9.7	3.7	17.5	16.6	5.4	9.7

volume entropy [43]. Therefore a high  $S$  may be due to a low energy requirement for CO<sub>2</sub> molecules to be introduced into polymer cavities.

Table 6 displays the gas transport properties of polyphenylene's evaluated for He, H<sub>2</sub>, O<sub>2</sub>, CO<sub>2</sub>, N<sub>2</sub> and CH<sub>4</sub> measured at 25 °C using a feed pressure of 4 atm. For the gas with the lowest condensability and KD, He diffusivity had a direct relationship with block length. For the other gases, all copolymers exhibited higher diffusivities and permeability's than the homopolymers. Gas solubility for the most condensable gas, CO<sub>2</sub>, increased with increasing methyl *-mer* length within multi-block and random copolymers. The highest and lowest gas solubility's were present in PP and MPP, and the copolymers were roughly an average of the two homopolymers. This indicates that incorporation of the methyl moiety effectively disrupts favorable gas-binding interactions that will reduce gas solubility. Fig. 9 displays gas  $P$ ,  $D$ , and  $S$  as a function of the diffraction angle of the d-1 peak. A decrease in solubility with

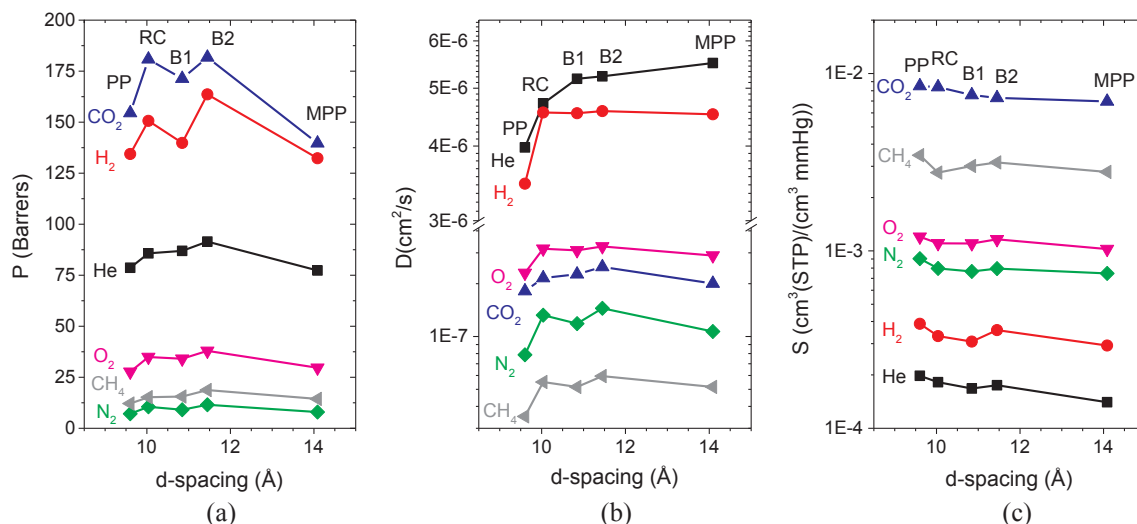


Fig. 9.  $P$ ,  $D$ ,  $S$ , and  $\alpha$  as a function of  $d$ -spacing of the amorphous feature.

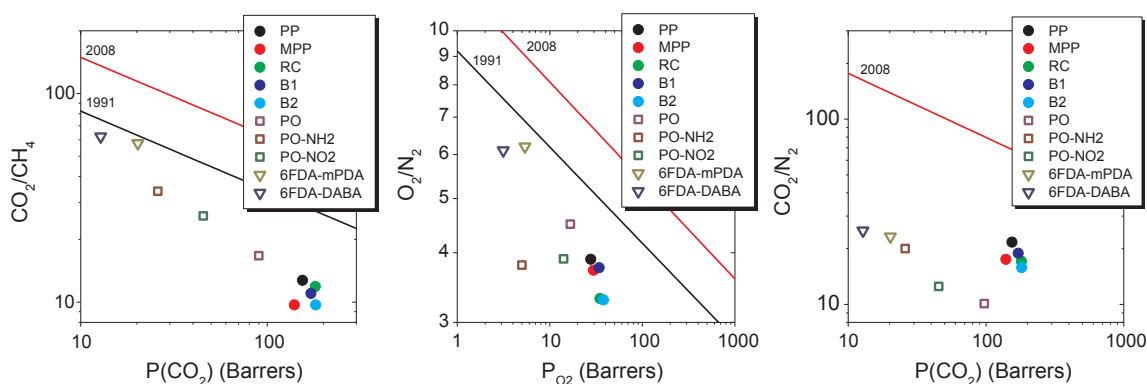


Fig. 10. The effect of chemical structure and morphology on the permeability/selectivity trade off of Diels-Alder poly(phenylene)s, modified POs [18,33], and 6FDA based polyimides [48].

$d$ -spacing is observed, most evident for the gas with the highest solubility, carbon dioxide. For the gasses with the lowest condensability, helium and hydrogen,  $D$  increases with  $d$ -spacing. These observations suggest a relationship between amorphous region ordering and gas transport properties that indicates  $S$  and  $D$  tune-ability.

The permselectivity of Diels-Alder poly(phenylene)s for  $\text{CO}_2/\text{CH}_4$  vs.  $P(\text{CO}_2)$ ,  $\text{O}_2/\text{N}_2$  vs.  $P(\text{O}_2)$  and  $\text{CO}_2/\text{N}_2$  vs.  $P(\text{CO}_2)$  with the Robson 1991 and 2008 upper bounds are shown in Fig. 10. Despite similar chemistries, the Diels-Alder poly(phenylene)s display a relatively high degree of variation in permselectivity. In addition, the permselectivity trade-off does not correlate well to polymer chemistry or composition, but depends largely on the gas pair. As previously discussed, this is due to different polymer microstructures that can be correlated to gas solubility and diffusivity. Reference materials in Fig. 10 include 6FDA based polyimides that have received considerable attention due to high gas permeabilities and selectivity's, which gives them industrial applicability [44]. The polymer most comparable in performance to Diels-Alder poly(phenylene)s is poly(phenylene oxide) (PO), which displays high gas  $P$  and moderate  $\alpha$ . Many chemical and physical modifications have been performed to improve the selectivity of PO including bromination [18], sulfonation [45], polymer blending [46], nitration and amination [33], and silica composites [47]. With similar modifications, Diels-Alder poly(phenylene)s could prove to be competitive candidates for industrial gas separation processes.

#### 4. Conclusions

Diels-Alder poly(phenylene) methylation and block copolymerization has a significant effect on the spatial conformation of polymer chains within a membrane. This was observed in changes of the X-ray diffraction amorphous peak, also referred to as the "polymerization peak." The membranes displayed narrow FFV's from 0.288 to 0.304. An increase in methylated block length increased the materials measured specific volume, decreased the glass transition temperature, and corresponded well to an increase in  $d$ -spacing of the amorphous peak. Increasing methyl block length was found to reduce gas solubility, yet increase diffusivity. These observations suggested that the methyl moiety disrupts chain packing causing an increase in void spacing, as well as reduces solubility by hindering gas-binding interactions. In general, Diels-Alder poly(phenylene)s permselective properties lie near the upper

bound, displaying high permeability and moderate selectivity. This work suggests that order within the amorphous region possesses some correlation to polymer chemistry, morphology, and gas transport properties.

## References

- [1] F.G. Kerry, *Industrial Gas Handbook: Gas Separation and Purification*, Taylor and Francis Group, LLC, 2006.
- [2] Y.-W. Jeon, D.-H. Lee, Gas membranes for CO<sub>2</sub>/CH<sub>4</sub> (Biogas) separation: a review, *Environ. Eng. Sci.* 32 (2015) 1–15.
- [3] S. Sridhar, B. Smitha, T.M. Aminabhavi, Separation of carbon dioxide from natural gas mixtures through polymeric membranes—a review, *Sep. Purif. Rev.* 36 (2007) 113–174.
- [4] P. Bernardo, E. Drioli, G. Golemme, Membrane gas separation: a review/state of the art, *Ind. Eng. Chem. Res.* 48 (2009) 4638–4663.
- [5] Y. Zhang, J. Sunarso, S. Liu, R. Wang, Current status and development of membranes for CO<sub>2</sub>/CH<sub>4</sub> separation: a review, *Int. J. Greenh. Gas Control* 12 (2013) 84–107.
- [6] D. Aaron, C. Tsouris, Separation of CO<sub>2</sub> from flue gas: a review, *Sep. Sci. Technol.* 40 (2005) 321–348.
- [7] Y.K. Ovchinnikov, E.M. Antipov, G.S. Markova, N.F. Bakeev, Comparative investigation of short-range order in unbranched alkanes and polyethylene, *Die Makromol. Chemie* 177 (1976) 1567–1581.
- [8] Geoffrey R. Mitchell, A.H.W. Richard Lovell, The local structure of molten polyethylene, *Polymer* 23 (1982) 12731285.
- [9] R.L. Miller, R.F. Boyer, Regularities in x-ray scattering patterns from amorphous polymers, *J. Polym. Part B Polym. Phys.* 22 (1984) 2043–2050.
- [10] R.L. Miller, R.F. Boyer, J. Heijboer, X-ray scattering from amorphous acrylate and methacrylate polymers: evidence of local order, *J. Polym. Sci. Part B Polym. Phys.* 22 (1984) 2021–2041.
- [11] Y. Hirayama, T. Yoshinaga, Y. Kusuki, K. Ninomiya, T. Sakakibara, T. Tamari, Relation of gas permeability with structure of aromatic polyimides I, *J. Memb. Sci.* 111 (1996) 169–182.
- [12] J.S. McHattie, W.J. Koros, D.R. Paul, Gas transport properties of polysulphones: 1. Role of symmetry of methyl group placement on bisphenol rings, *Polymer (Guildf)* 32 (1991) 840–850.
- [13] K.C. Khulbe, T. Matsuura, G. Lamarche, a.-M. Lamarche, X-ray diffraction analysis of dense PPO membranes, *J. Memb. Sci.* 170 (2000) 81–89.
- [14] S. Park, K. Kim, W. So, S. Moon, S. Lee, Gas separation properties of 6FDA-based polyimide membranes with a polar group, *Macromol. Res.* 11 (2003) 157–162.
- [15] I. Tanis, D. Brown, S.J. Neyertz, R. Heck, R. Mercier, A comparison of homopolymer and block copolymer structure in 6FDA-based polyimides, *Phys. Chem. Chem. Phys.* 16 (2014) 23044–23055.
- [16] C. Cornelius, Hybrid inorganic–organic materials based on a 6FDA–6FpDA–DABA polyimide and silica: physical characterization studies, *Polymer (Guildf)* 43 (2002) 2385–2400.
- [17] S.S. Hosseini, M.M. Teoh, T.S. Chung, Hydrogen separation and purification in membranes of miscible polymer blends with interpenetration networks, *Polymer (Guildf)* 49 (2008) 1594–1603.
- [18] F. Hamad, T. Matsuura, Performance of gas separation membranes made from sulfonated brominated high molecular weight poly(2,4-dimethyl-1,6-phenylene oxide), *J. Memb. Sci.* 253 (2005) 183–189.
- [19] M. Hibbs, C. Fujimoto, C. Cornelius, Synthesis and characterization of poly(phenylene)-based anion exchange membranes for alkaline fuel cells, *Macromolecules* 42 (2009) 8316–8321.
- [20] R.J. Stanis, et al., Evaluation of hydrogen and methanol fuel cell performance of sulfonated diels alder poly(phenylene) membranes, *J. Power Sources* 195 (2010) 104–110.
- [21] C. Fujimoto, S. Kim, R. Stains, X. Wei, Vanadium redox flow battery efficiency and durability studies of sulfonated Diels Alder poly(phenylene)s, *Electrochem. Ellipsis* 20 (2012) 48–51.
- [22] A.J. Berresheim, M. Müller, K. Müllen, Polyphenylene nanostructures, *Chem. Rev.* 99 (1999) 1747–1785.
- [23] U. Kumar, T. Neenan, Diels-Alder polymerization between bis(cyclopentadienones) and acetylenes. A versatile route to new highly aromatic polymers, *Macromolecules* 28 (1995) 124–130.
- [24] C.H. Fujimoto, M.A. Hickner, C.J. Cornelius, D.A. Loy, Ionomeric poly(phenylene) prepared by Diels - Alder polymerization: synthesis and physical properties of a novel polyelectrolyte, *Macromolecules* (2005) 5010–5016.
- [25] M. Ogliaruso, E. Becker, Bistetracyclones and Bishexaphenylbenzenes. II, *J. Org. Chem.* 30 (1965) 3354–3360.
- [26] A.A. Bondi, Physical properties of molecular crystals liquids, and glasses. *J. Appl. Polym. Sci.* (1968).
- [27] D.W. Van Krevelen, K. Te Nijenhuis, *Properties of Polymers: Their Correlation with Chemical Structure; Their Numerical Estimation and Prediction from Additive Group Contributions*, Elsevier Sci. Publ. (Elsevier), 2009.
- [28] J. Alexopoulos, J. Barrie, D. Machin, The time lag for the diffusion of gas mixtures, *Polymer (Guildf)* 10 (1969) 265–269.
- [29] J. Stille, G. Noren, Catenation and kinetics of the Diels-Alder step-growth reaction in the synthesis of phenylated polyphenylenes, *Macromolecules* 5 (1972).
- [30] Z.B. Shifrina, M.S. Averina, A.L. Rusanov, M. Wagner, K. Mu, Branched polyphenylenes by repetitive Diels - Alder cycloaddition, *Macromolecules* 3525–3529 (2000).
- [31] W. Qu, T.M. Ko, R.H. Vora, T.S. Chung, Effect of polyimides with different ratios of para- to meta- analogous fluorinated diamines on relaxation process, *Polymer (Guildf)* 42 (2001) 6393–6401.
- [32] M. Oroujzadeh, S. Mehdipour-Ataei, M. Esfandeh, Preparation and properties of novel sulfonated poly(arylene ether ketone) random copolymers for polymer electrolyte membrane fuel cells, *Eur. Polym. J.* 49 (2013) 1673–1681.
- [33] Y.S. Bhole, P.B. Karadkar, U.K. Kharul, Nitration and amination of polyphenylene oxide: synthesis, gas sorption and permeation analysis, *Eur. Polym. J.* 43 (2007) 1450–1459.
- [34] C.L. Aitken, W.J. Koros, D.R. Paul, Gas transport properties of biphenol polysulfones, *Macromolecules* 25 (1992) 3651–3658.
- [35] J. Stille, R.O. Rakutis, H. Mukamal, F.w. Harris, Diels-alder polymerizations. IV. Polymers containing short phenylene blocks connected by alkylene units, *Macromolecules* 1 (1968) 431–436.
- [36] L.a. Wall, Pyrolysis of polymers, *J. Elastomers Plast.* 5 (1973) 36–65.
- [37] H.R. Schubach, E. Nagy, B. Heise, Short range order of amorphous polymers derived by WAXS, *Colloid Polym. Sci.* 259 (1981) 789–796.
- [38] J.R. Katz, X-ray spectrography of polymers and in particular those having a rubber-like extensibility, *Rubber Chem. Technol.* 9 (1936) 357–372.
- [39] G.R. Mitchell, A.H. Windle, Structure of polystyrene glasses, *Polymer (Guildf)* 25 (1984) 906–920.
- [40] C. Ayyagari, D. Bedrov, G.D. Smith, Structure of atactic polystyrene: a molecular dynamics simulation study, *Macromolecules* 33 (2000) 6194–6199.
- [41] K. Okamoto, K. Tanaka, M. Katsube, H. Kita, O. Sueoka, Ito, Correlation between positron annihilation and gas diffusion properties of various rubbery polymers, *Polym J* 25 (1993) 275–284.
- [42] G.M. Geise, C.M. Doherty, A.J. Hill, B.D. Freeman, D.R. Paul, Free volume characterization of sulfonated styrenic pentablock copolymers using positron annihilation lifetime spectroscopy, *J. Memb. Sci.* 453 (2014) 425–434.
- [43] N.F.A. Van der Vegt, V.A. Kusuma, B.D. Freeman, Basis of solubility versus TC correlations in polymeric gas separation membranes, *Macromolecules* 43 (2010) 1473–1479.
- [44] K.J. Kim, S.H. Park, W.W. So, D.J. Ahn, S.J. Moon, CO<sub>2</sub> separation performances of composite membranes of 6FDA-based polyimides with a polar group, *J. Memb. Sci.* 211 (2003) 41–49.
- [45] J. Rhim, G. Chowdhury, T. Matsuura, Development of thin-film composite membranes for carbon dioxide and methane separation using sulfonated poly(phenylene oxide), *J. Appl. Polym. Sci.* 735–742 (1999).
- [46] Y. Maeda, D.R. Paul, Selective gas transport in miscible PPO-PS blends, *Polymer (Guildf)* 26 (1985) 2055–2063.
- [47] B. Yu, H. Cong, X. Zhao, Hybrid brominated sulfonated poly(2,6-diphenyl-1,4-phenylene oxide) and SiO<sub>2</sub> nanocomposite membranes for CO<sub>2</sub>/N<sub>2</sub> separation, *Prog. Nat. Sci. Mater. Int.* 22 (2012) 661–667.
- [48] W. Qiu, L. Xu, C.-C. Chen, D.R. Paul, W.J. Koros, Gas separation performance of 6FDA-based polyimides with different chemical structures, *Polymer (Guildf)* 54 (2013) 6226–6235.